J|A|C|S ARTICLES

Published on Web 11/10/2010

Leaving Group Activation and Pyrophosphate Ionic State at the Catalytic Site of *Plasmodium falciparum* Orotate Phosphoribosyltransferase

Yong Zhang, Hua Deng, and Vern L. Schramm*

Department of Biochemistry, Albert Einstein College of Medicine, 1300 Morris Park Avenue, Bronx, New York 10461, United States

Received August 30, 2010; E-mail: vern.schramm@einstein.yu.edu

Abstract: *Plasmodium falciparum* orotate phosphoribosyltransferase (*Pf*OPRT) catalyzes the reversible pyrophosphorolysis of orotidine 5′-monophosphate (OMP). Transition-state analysis from kinetic isotope effects supports a dianionic orotic acid (OA) leaving group. Isotope-edited Fourier transform infrared (FTIR) spectrometry complemented by homology modeling and quantum chemical calculations were used to characterize the orotate hydrogen-bond network for *Pf*OPRT. Bond stretch frequencies for C_2═O and C_4═O of OMP were established from ^{13}C-edited FTIR difference spectra. Both frequencies were shifted downward by 20 cm^{-1} upon formation of the Michaelis complex. Hydrogen-bond interactions to the orotate moiety induce strong leaving group polarization by ground-state destabilization. The C_2═O bond is 2.7 Å from two conserved water molecules, and the C_4═O bond is within 2.4 Å of the $NH_2(\omega)$ of Arg241 and the peptide NH of Phe97. Relative to free OMP, the N1 atom of *Pf*OPRT-bound OMP indicates a ΔpK_a of −4.6. The decreased basicity of N1 supports leaving group activation through a hydrogen-bond network at the *Pf*OPRT active site. *Pf*OPRT in complex with ^{18}O−PPi and a proposed transition-state analogue revealed a trianionic PPi nucleophile with no significant P··O bond polarization, supporting a mechanism proceeding through the migration of the ribocation toward the PPi. These results along with previous *Pf*OPRT transition-state analyses provide reaction coordinate information for the *Pf*OPRT-catalyzed OMP pyrophosphorolysis reaction.

Introduction

De novo pyrimidine biosynthesis requires six sequential enzymatic reactions to generate uridine 5′-monophosphate (UMP). As the fifth enzyme in this pathway, orotate phosphoribosyltransferase (OPRT; EC 2.4.2.10) catalyzes the reversible formation of orotidine 5′-monophosphate (OMP) and pyrophosphate (PPi) from α-D-phosphoribosylpyrophosphate (PRPP) and orotate (Figure 1). OMP is subsequently converted by OMP decarboxylase to UMP, serving as the precursor for all pyrimidine nucleotides used in cellular metabolism, DNA and RNA synthesis. *Plasmodium falciparum*, the most virulent protozoan parasite responsible for malaria, requires de novo pyrimidine biosynthesis and lacks the enzymes for pyrimidine salvage.[1−3] *P. falciparum* OPRT (*Pf*OPRT) is thus an essential enzyme in the parasites.[4−6] The *Pf*OPRT kinetic mechanism follows a random sequential pattern for both the forward and the reverse reactions.[7] Inhibitors disrupting de novo pyrimidine biosynthesis show antimalarial potency in *P. falciparum* parasites.[7−10]

Transition-state analyses from isotope effects and quantum chemical calculations reveal the *Pf*OPRT transition state to be a fully dissociated, dianionic orotic acid (OA) with a well-developed ribocation and weak participation of the pyrophosphate nucleophile.[11,12] Most *N*-ribosyltransferase transition states involve protonated, neutral leaving groups at the transition state. The *Pf*OPRT transition state is unexpected since the unprotonated (dianionic) OA makes a poor leaving group from the cationic transition state. Poor substrate activity of *Pf*OPRT with *p*-nitrophenyl β-D-ribose 5′-monophosphate supports leaving group activation as a major catalytic force for OMP pyrophosphorolysis.[11] No crystal structure is available for *Pf*OPRT, but structures of related OPRTs from *Salmonella typhimurium* and *Saccharomyces cerevisiae* permit homology modeling.[13,14] At these active sites, enzyme-bound OMPs form extensive hydrogen-

(1) Gero, A. M.; O'Sullivan, W. J. *Blood Cells* **1990**, *16*, 467–484.
(2) Jones, M. E. *Annu. Rev. Biochem.* **1980**, *49*, 253–279.
(3) Reyes, P.; Rathod, P. K.; Sanchez, D. J.; Mrema, J. E.; Rieckmann, K. H.; Heidrich, H. G. *Mol. Biochem. Parasitol.* **1982**, *5*, 275–290.
(4) Queen, S. A.; Jagt, D. L.; Reyes, P. *Antimicrob. Agents Chemother.* **1990**, *34*, 1393–1398.
(5) Rathod, P. K.; Khatri, A.; Hubbert, T.; Milhous, W. K. *Antimicrob. Agents Chemother.* **1989**, *33*, 1090–1094.
(6) Scott, H. V.; Gero, A. M.; O'Sullivan, W. J. *Mol. Biochem. Parasitol.* **1986**, *18*, 3–15.
(7) Krungkrai, S. R.; Aoki, S.; Palacpac, N. M.; Sato, D.; Mitamura, T.; Krungkrai, J.; Horii, T. *Mol. Biochem. Parasitol.* **2004**, *134*, 245–255.
(8) Krungkrai, J.; Krungkrai, S. R.; Phakanont, K. *Biochem. Pharmacol.* **1992**, *43*, 1295–1301.
(9) Phillips, M. A.; Gujjar, R.; Malmquist, N. A.; White, J.; El Mazouni, F.; Baldwin, J.; Rathod, P. K. *J. Med. Chem.* **2008**, *51*, 3649–3653.
(10) Seymour, K. K.; Lyons, S. D.; Phillips, L.; Rieckmann, K. H.; Christopherson, R. I. *Biochemistry* **1994**, *33*, 5268–5274.
(11) Zhang, Y.; Luo, M.; Schramm, V. L. *J. Am. Chem. Soc.* **2009**, *131*, 4685–4694.
(12) Zhang, Y.; Schramm, V. L. *J. Am. Chem. Soc.* **2010**, *132*, 8787–8794.

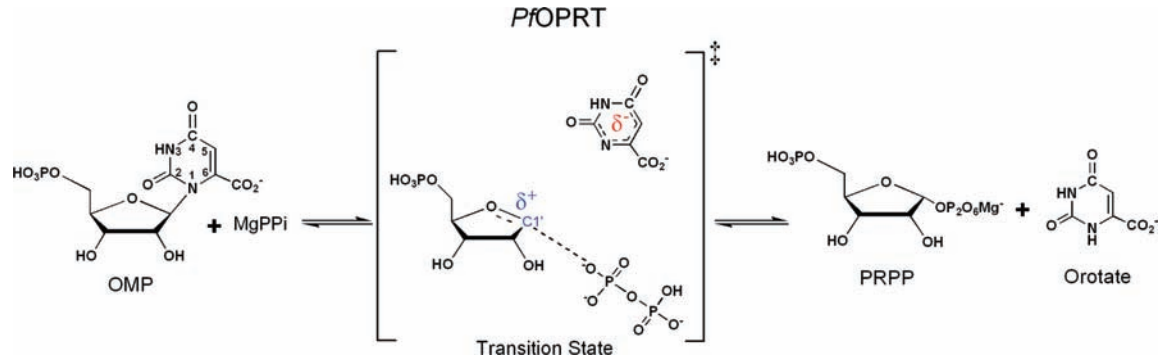

Figure 1. *Pf*OPRT-catalyzed reversible OMP pyrophosphorolysis.

bond interactions with surrounding residues and ordered water molecules and the conserved active site residues suggest a similar catalytic architecture for *Pf*OPRT. Results from the transition-state analyses, substrate specificity, and crystal structures support a reaction coordinate with activation of the OA leaving group through multiple hydrogen-bond interactions at the *Pf*OPRT active site.

Infrared spectral analysis of human purine nucleoside phosphorylase (PNP) in complex with phosphate and Immucillin-H, a transition-state analogue, has been used to reveal a highly activated phosphate dianion with distorted P••O bonds at the catalytic site.[15] A similar study of human hypoxanthine-guanine phosphoribosyltransferase (HGPRT) shows an enzyme-bound PPi tetraanion with no significant P••O bond polarization.[16] Isotope-edited Fourier transform infrared (FTIR) spectrometry provides unique bonding insight[17−23] and was used here to explore the nature of pyrophosphate at the catalytic site of *Pf*OPRT. Incorporating isotopes at specific atomic positions permits assignments of the vibrational bands in IR spectrum, and bond frequency is diagnostic of the electronic environment of specific bonds.[24]

Here, ^{13}C-edited FTIR difference spectrometry is complemented by homology modeling and quantum chemical calculations to establish the hydrogen-bond network at the *Pf*OPRT active site. Spectra for OMP in solution and in the Michaelis complex indicate strong hydrogen bonds between orotate and the active site residues. Computational matching of frequency shifts supports a hydrogen-bond network to OA oxygens and a decreased pK_a of OMP, supporting OA leaving group activation by multiple hydrogen-bond interactions. *Pf*OPRT in complex with MgPPi and a proposed transition-state analogue revealed a trianionic PPi nucleophile with no significant bond polarization beyond that of the binary complex of *Pf*OPRT with MgPPi. These features support a mechanism proceeding through ribocation migration toward the PPi nucleophile.

Experimental Methods

Reagents and Materials. DL-[4-^{13}C]Aspartic acid and [^{13}C]urea were purchased from Cambridge Isotope Laboratories. [^{18}O]Water (99 atom % ^{18}O), adenylate kinase (AK), and pyruvate kinase (PK) were purchased from Sigma-Aldrich. Phospho-D-ribosyl-α-1-pyrophosphate synthase (PRPPase) and ribokinase (RK) were prepared as described before.[25,26] *Pf*OPRT was expressed in *E.coli* cells and purified as described previously.[11] All other reagents were purchased from readily available commercial sources and used without further purification. Carbon nuclear magnetic resonance (^{13}C NMR) chemical shifts were measured in DMSO-d_6 using a Bruker 300 MHz instrument. The ^{13}C NMR spectra were collected using continuous proton-decoupling mode with at least 10 000 scans. Mass spectra were acquired on an IonSpec FT-ICR mass spectrometer (Varian Inc., CA).

Synthesis of [2-^{13}C]OMP and [4-^{13}C]OMP. [2-^{13}C]Orotic acid and [4-^{13}C]orotic acid were prepared from [^{13}C]urea and DL-[4-^{13}C]aspartic acid, respectively.[11] [2-^{13}C]Orotic acid: ^{13}C NMR (75 MHz, DMSO-d_6) δ ppm 152; *m/z* std $C_5H_5N_2O_4$ (M + 1) 157.026, $C_4{}^{13}C_1H_5N_2O_4$ (M + 1) 158.028. [4-^{13}C]Orotic acid: ^{13}C NMR (75 MHz, DMSO-d_6) δ ppm 165; *m/z* std $C_5H_5N_2O_4$ (M + 1) 157.026, $C_4{}^{13}C_1H_5N_2O_4$ (M + 1) 158.028. [2-^{13}C]OMP and [4-^{13}C]OMP were prepared enzymatically with the [2-^{13}C]orotic acid and [4-^{13}C]orotic acid as precursors.[11]

Synthesis of [$^{18}O_7$]PPi. [$^{18}O_7$]PPi was prepared with a 5:1 molar ratio of H_2O:PCl_5.[27] The PPi product was purified twice using AG1-X4 resin (100−200 mesh, Cl^-, Bio-Rad., Hercules, CA), with elution by 150 mM HCl. [$^{18}O_7$]PPi: *m/z* std $HK_4O_7P_2$ (M + 1) 330.775, $HK_4{}^{18}O_7P_2$ (M + 1) 344.806; isotopic purity [$^{18}O_7$]PPi >97%.

Isotope-Edited FTIR Difference Spectroscopy. FTIR spectroscopy was performed on a Magna 760 Fourier transform spectrometer (Nicolet Instrument Corp., WI) with an MCT (mercury−cadmium−telluride) detector. Labeled and unlabeled samples were simultaneously loaded into a two-position dual-cell shuttle accessory. FTIR spectra were collected alternatively between labeled and unlabeled samples. Purified *Pf*OPRT and ^{13}C-labeled OMPs were prepared in D_2O-based buffer for ^{13}C-edited FTIR measurements by using CaF_2 windows with 25 μm Teflon spacers. The concentrations of *Pf*OPRT and OMP were both 3.8 mM. With

(13) Gonzalez-Segura, L.; Witte, J. F.; McClard, R. W.; Hurley, T. D. *Biochemistry* **2007**, *46*, 14075–14086.
(14) Scapin, G.; Grubmeyer, C.; Sacchettini, J. C. *Biochemistry* **1994**, *33*, 1287–1294.
(15) Deng, H.; Lewandowicz, A.; Schramm, V. L.; Callender, R. *J. Am. Chem. Soc.* **2004**, *126*, 9516–7.
(16) Deng, H.; Callender, R.; Schramm, V. L.; Grubmeyer, C. *Biochemistry* **2010**, *49*, 2705–14.
(17) Deng, H.; Murkin, A. S.; Schramm, V. L. *J. Am. Chem. Soc.* **2006**, *128*, 7765–71.
(18) Deng, H.; Brewer, S.; Vu, D. M.; Clinch, K.; Callender, R.; Dyer, R. B. *Biophys. J.* **2008**, *95*, 804–13.
(19) Du, X.; Frei, H.; Kim, S. H. *J. Biol. Chem.* **2000**, *275*, 8492–500.
(20) Mertz, E. L.; Leikin, S. *Biochemistry* **2004**, *43*, 14901–12.
(21) Martinez-Liarte, J. H.; Iriarte, A.; Martinez-Carrion, M. *Biochemistry* **1992**, *31*, 2712–9.
(22) Chakrabarti, P. P.; Suveyzdis, Y.; Wittinghofer, A.; Gerwert, K. *J. Biol. Chem.* **2004**, *279*, 46226–33.
(23) Cheng, H.; Sukal, S.; Deng, H.; Leyh, T. S.; Callender, R. *Biochemistry* **2001**, *40*, 4035–43.
(24) Callender, R.; Deng, H. *Annu. Rev. Biophys. Biomol. Struct.* **1994**, *23*, 215–45.
(25) Parkin, D. W.; Leung, H. B.; Schramm, V. L. *J. Biol. Chem.* **1984**, *259*, 9411–9417.
(26) Singh, V.; Lee, J. E.; Nunez, S.; Howell, P. L.; Schramm, V. L. *Biochemistry* **2005**, *44*, 11647–11659.
(27) Hackney, D. D.; Stempel, K. E.; Boyer, P. D. *Methods Enzymol.* **1980**, *64*, 60–83.

a K_m of 3.7 μM for *Pf*OPRT, more than 97% OMP was bound to the *Pf*OPRT. The FTIR spectra were collected in the range of 1100−4000 cm^{-1} with 2 cm^{-1} resolution. For ^{18}O-edited FTIR measurements, BaF_2 windows with 25 μm Teflon spacers were used to collect spectra in the range of 900−4000 cm^{-1} with 2 cm^{-1} resolution. A Blackman-Harris three-term apodization and a Happ−Genzel apodization were applied, respectively. Omnic 4.1a (Nicolet Instrument Corp.) software was used to collect and analyze FTIR spectra. Due to the different path lengths in cells for labeled and unlabeled samples, resulting from separate assembly, the subtracted spectra were normalized with a correction factor, usually in the range of 0.95−1.05.

Homology Modeling of *Pf*OPRT. The structural model of *Pf*OPRT (residues 64−278) was generated by SWISS-MODEL (http://swissmodel.expasy.org/) with *S. cerevisiae* OPRT (*Sc*OPRT) crystal structure as template (PDB code 2PS1, chain B).[13,28−30]

Quantum Chemical Calculations. The hydrogen-bond network at the *Pf*OPRT catalytic site was modeled in vacuo using hybrid density functional theory implemented in Gaussian 03.[31] 1-Methyl OA was used as the OMP mimic. On the basis of the *Pf*OPRT homology model, active site residues or water molecules in hydrogen bonds to the orotate moiety were included for calculations. Geometry optimizations were performed at the B3LYP/6-31G(d,p) level for enzyme-bound 1-methyl OA with varied hydrogen-bond distances to the C_2═O and C_4═O bonds. Vibrational frequencies were calculated at the same level of theory and basis set. With experimental carbonyl stretching frequency shifts as boundary conditions, the hydrogen-bond distances were iteratively altered to generate models providing the best match.

Computation of a hydrogen-bond network in solution used the self-consistent reaction field (SCRF) method using an Onsager model implemented in Gaussian 03.[32−34] Geometries of the *Pf*OPRT active site with bound 1-methyl OA were optimized and calculated for vibrational frequencies using the dielectric environment of water. The recommended radii for calculations in water were determined with the Vol key word in the route section.

Natural bond orbital (NBO) analyses were performed on the optimized geometries by adding the pop═nbo key word in the route section. Molecular electrostatic potential (MEP) surfaces were generated using the CUBE subprogram from Gaussian 03. Formatted checkpoint files from geometry optimization were used as inputs. The MEP surfaces were visualized at an isovalue of 0.1 using GaussView 3.09.[31]

Computational analyses of the decrease in pK_a at N1 of 1-methyl OA upon formation of the Michaelis complex were carried out in vacuo and in water. Standard correlation curves were generated by plotting energetic differences between protonated and unprotonated base groups versus their corresponding pK_a values of N1 atoms.[35,36] For uracil and OA with various protonation states, geometry optimizations and frequency calculations were performed in vacuo and in water at the B3LYP/6-31G(d,p) level. The calculations in water were carried out by the SCRF method in the Onsager model implemented in Gaussian 03. The recommended radii were obtained through volume calculations.

Calculations for PPi with various ionic states were performed at the B3LYP/6-31G(d,p) level. Geometries of di-, tri-, and tetraanionic PPi were optimized without constraints. Vibrational frequencies were subsequently calculated at the same level of theory and basis set.

Results and Discussion

^{13}C-Edited FTIR Difference Spectra of OMP. Isotope-edited FTIR difference spectra reflect vibrational differences between isotopically labeled and unlabeled compounds. By incorporating an isotope into the bond of interest, vibrational frequencies for the corresponding bond are altered and appear as vibrational shifts in the FTIR difference spectrum. Difference spectra permit assignments of vibrational modes of interest, since all other irrelevant modes are subtracted in the difference spectra.

Carbonyl stretching frequencies of C_2═O and C_4═O bonds for OMP in solution were determined from ^{13}C-edited FTIR difference spectra by using [2-^{13}C]OMP and [4-^{13}C]OMP, respectively. The stretching frequency of the C_2═O bond is 1660 cm^{-1}, showing a shift of −18 cm^{-1} upon ^{13}C labeling (Figure 2). The C_4═O bond has a stretching frequency of 1658 cm^{-1} in solution and decreases by 20 cm^{-1} upon ^{13}C labeling (Figure 2). For free OMP in solution, the stretching frequencies of C_2═O and C_4═O bonds are similar and located in the range of amide C═O stretching (1630−1690 cm^{-1}).

^{13}C-Edited FTIR Difference Spectra of *Pf*OPRT-Bound OMP. Stretching frequencies of the C_2═O and C_4═O bonds for enzyme-bound OMP were determined from ^{13}C-edited FTIR difference spectra (Figure 2). By subtracting the FTIR spectrum of *Pf*OPRT:unlabeled-OMP from that of *Pf*OPRT:^{13}C-labeled OMP, vibrational bands arising from the protein are eliminated. The C_2═O stretch frequency in the Michaelis complex is 1640 cm^{-1} and shifts to 1622 cm^{-1} upon ^{13}C labeling (Figure 2). For the C_4═O bond of *Pf*OPRT-bound OMP, the stretching frequencies are 1638 and 1616 cm^{-1} for unlabeled and labeled OMP, respectively (Figure 2). Compared to their frequencies in solution, C_2═O and C_4═O bonds both display a frequency shift of −20 cm^{-1} in the Michaelis complex (Table 1). These downward shifts indicate formation of favorable hydrogen bonds between orotate and the catalytic site. Transition-state analysis indicates that *Pf*OPRT-catalyzed OMP pyrophosphorolysis proceeds through an unprotonated (dianionic) OA leaving group. Therefore, multiple hydrogen-bond interactions at the *Pf*OPRT active site, as reflected from the ^{13}C-edited FTIR difference spectra, are anticipated to play an important role in activating the leaving group (see below).

Homology Modeling of *Pf*OPRT Structure. A *Pf*OPRT structural model was generated using SWISS-MODEL with the *Sc*OPRT crystal structure as a template (PDB code 2PS1, chain B). The homology structure of *Pf*OPRT provided the basis for computational analysis (see below). Sequence alignment of OPRT homologues revealed that *Pf*OPRT contains the conserved active site residues in addition to a unique N-terminal (60 amino acids) insertion. This N-terminal insertion is speculated to be involved in formation of a heterotetramer with *P. falciparum* OMP decarboxylase.[37] Sequence alignment between *Pf*OPRT (residues 64−278) and *Sc*OPRT showed a sequence identity of 31%. The homology structure of *Pf*OPRT is composed of 7 α-helices and 11 β-strands, with a core characterized by a 5-stranded parallel β-sheet, surrounded by 4 α-helices. The overall fold of *Pf*OPRT is similar to those of *Escherichia coli*, *S. typhimurium*, and *S. cerevisiae* OPRT.[13,14,38]

(28) Arnold, K.; Bordoli, L.; Kopp, J.; Schwede, T. *Bioinformatics* **2006**, *22*, 195–201.
(29) Schwede, T.; Kopp, J.; Guex, N.; Peitsch, M. C. *Nucleic Acids Res.* **2003**, *31*, 3381–5.
(30) Guex, N.; Peitsch, M. C. *Electrophoresis* **1997**, *18*, 2714–2723.
(31) Frisch, M. J. Gaussian, Inc.: Wallingford, CT, 2004.
(32) Onsager, L. *J. Am. Chem. Soc.* **1936**, *58*, 1486–1493.
(33) Wong, M. W.; Wiberg, K. B.; Frisch, M. *J. Chem. Phys.* **1991**, *95*, 8991–8998.
(34) Wong, M. W.; Frisch, M. J.; Wiberg, K. B. *J. Am. Chem. Soc.* **1991**, *113*, 4776–4782.
(35) Dawson, R. M. C.; Elliott, D. C.; Elliott, W. H.; Jones, K. M. *Data for Biochemical Research*; Clarendon Press: Oxford, 1959.
(36) Bendich, A. In *The Nucleic Acids: Chemistry and Biology*; Chargaff, E., Davidson, J. N., Eds.; Academic Press: New York, 1955; Vol. 1.
(37) Krungkrai, S. R.; DelFraino, B. J.; Smiley, J. A.; Prapunwattana, P.; Mitamura, T.; Horii, T.; Krungkrai, J. *Biochemistry* **2005**, *44*, 1643–1652.

Table 1. Experimental and Computationally Matched C=O Stretching Frequencies[a]

	C_2=O stretching frequencies (cm^{-1})			C_4=O stretching frequencies (cm^{-1})		
	free OMP in solution	*Pf*OPRT:OMP complex	shift[b]	free OMP in solution	*Pf*OPRT:OMP complex	shift
expt	1660 (1642)[d]	1640 (1622)	−20 (−20)	1658 (1638)	1638 (1616)	−20 (−22)
calcd in vacuo	1779 (1731)	1753 (1712)	−26 (−19)	1769 (1727)	1725 (1688)	−44 (−39)
calcd in water[c]	1785 (1744)	1765 (1725)	−20 (−19)	1754 (1716)	1734 (1696)	−20 (−20)

[a] Computationally matched C=O stretching frequencies were obtained by iteratively altering the specific hydrogen-bond distances within the *Pf*OPRT active site model. 1-Methyl OA was used as a simplified OMP for calculations. [b] Shift in the corresponding C=O stretch frequency changes of OMPs upon formation of the Michaelis complex. [c] Calculations in water were performed using the Onsager model implemented in Gaussian 03. [d] The numbers in parentheses are the stretching frequencies or frequency shift of corresponding ^{13}C-labeled C=O bond.

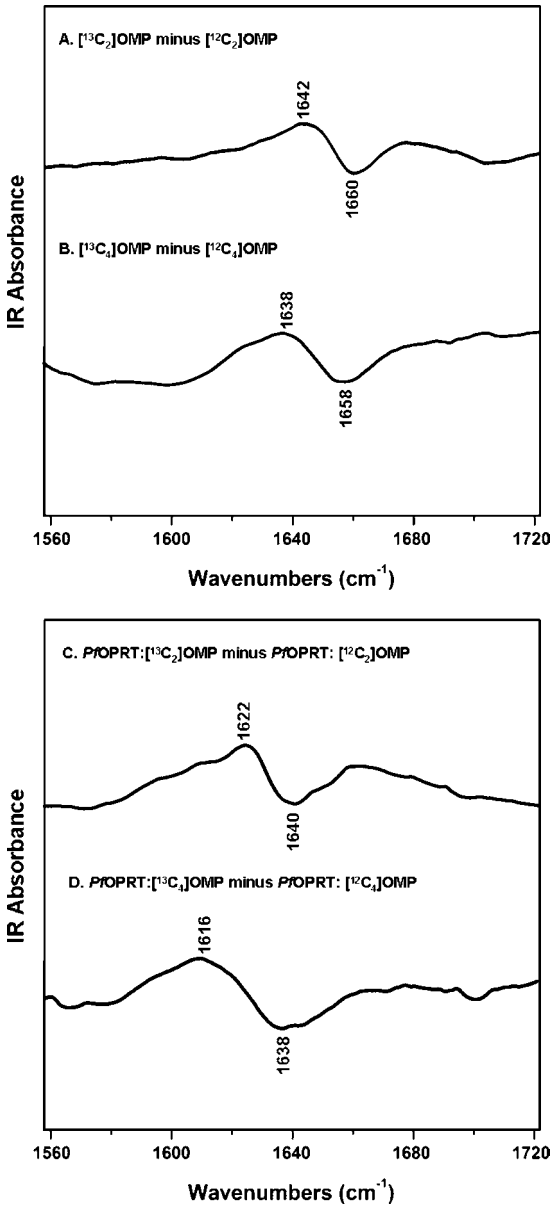

Figure 2. ^{13}C-edited FTIR difference spectra of OMP in solution (upper panel) and *Pf*OPRT·OMP (lower panel). (A) [$^{13}C_2$]OMP minus [$^{12}C_2$]OMP. (B) [$^{13}C_4$]OMP minus [$^{12}C_4$]OMP. OMPs were prepared in D_2O with a concentration of 3.8 mM. (C) *Pf*OPRT·[$^{13}C_2$]OMP minus *Pf*OPRT·[$^{12}C_2$]OMP. (D) *Pf*OPRT·[$^{13}C_4$]OMP minus *Pf*OPRT·[$^{12}C_4$]OMP. All samples were prepared in 50 mM Tris-HCl (pH = 8.0) and 200 mM NaCl in D_2O. The concentrations of *Pf*OPRT·OMP were both 3.8 mM.

A structural model of *Pf*OPRT in complex with OMP was built by merging the OMP from *Sc*OPRT structure (PDB code 2PRZ, chain A) into the aligned *Pf*OPRT homology structure. The active site of *Pf*OPRT consists of residues from the core and a catalytic loop (Figure 3A). An extended hydrogen-bond network is formed between orotate, surrounding residues, and water molecules (Figure 3B). The oxygen of C_2=O in OMP forms hydrogen bonds to two ordered water molecules. The N_3−H of OMP forms a hydrogen bond with the peptide C=O of Phe98, and the oxygen of C_4=O hydrogen bonds to the guanidinium of Arg241 and the peptide N−H of Phe97. The 6-carboxyl group of OMP forms multiple hydrogen bonds with the peptide N−H of Lys89, the side chain OH of Thr212, and two water molecules. These catalytic site residues are conserved throughout the OPRT family on the basis of sequence and structure alignment. The ordered water molecules forming hydrogen bonds to the orotate group are also recurrent features in OPRT crystal structures.[13,14,38,39]

The conserved hydrogen-bond network at the *Pf*OPRT active site causes downward shifts of the C_2=O and C_4=O carbonyl stretching frequencies upon formation of the Michaelis complex. Thus, multiple hydrogen-bond interactions are a major catalytic force for leaving group activation. The homology model of the *Pf*OPRT:OMP complex provided the basis for modeling the hydrogen-bond network by matching computational and experimental frequency shifts and elucidating the *Pf*OPRT catalytic mechanism (see below).

Computational Modeling of the Hydrogen-Bond Network in *Pf*OPRT. The catalytic site hydrogen-bond network was modeled computationally by matching calculated and experimental bond vibrational shifts. Calculations were performed in vacuo ($\varepsilon = 1$) and in water ($\varepsilon = 78.39$), representing two limits of the local dielectric environment of the *Pf*OPRT active site. An initial model for calculation was based on the active site geometry from a homology model of the *Pf*OPRT:OMP complex. 1-Methyl OA was used as a truncated model of OMP in these calculations. In addition to the 1-methyl OA, the computational model consists of all groups in hydrogen bonds to the orotate moiety, including backbones of Lys89, Phe97, and Phe98, side chains of Thr212 and Arg241, and four water molecules. These groups are within hydrogen-bond distance to the 2- and 4-carbonyls and the 6-carboxyl group of OMP. At the *Pf*OPRT active site, the phenyl ring of Phe97 is parallel to and stacked under the OA ring, with an interplanar distance of approximately 4 Å. Calculations with and without the phenyl ring had no effect on carbonyl and carboxyl vibrational frequencies. Thus, it was excluded for computational modeling. The hydrogen-bond network was modeled by iteratively altering distances of C_2=O to two water molecules and C_4=O to $NH_2(\omega)$ of Arg241 and NH of Phe97, with fixed non-hydrogen atoms of amino acid residues and water molecules.

(38) Henriksen, A.; Aghajari, N.; Jensen, K. F.; Gajhede, M. *Biochemistry* **1996**, *35*, 3803–3809.
(39) Scapin, G.; Ozturk, D. H.; Grubmeyer, C.; Sacchettini, J. C. *Biochemistry* **1995**, *34*, 10744–10754.

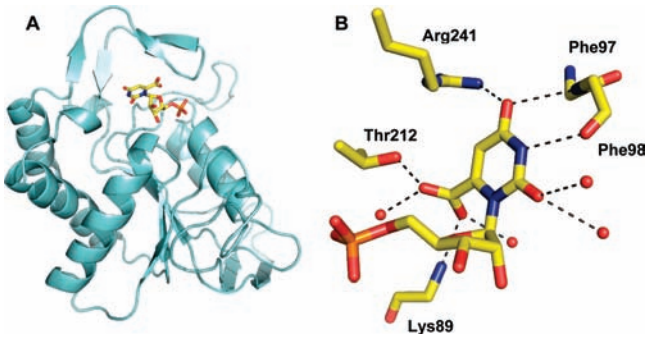

Figure 3. Homology model of *Pf*OPRT. (A) Overall structure of *Pf*OPRT in complex with OMP. (B) *Pf*OPRT active site with residues and water molecules in hydrogen bonds to the leaving group.

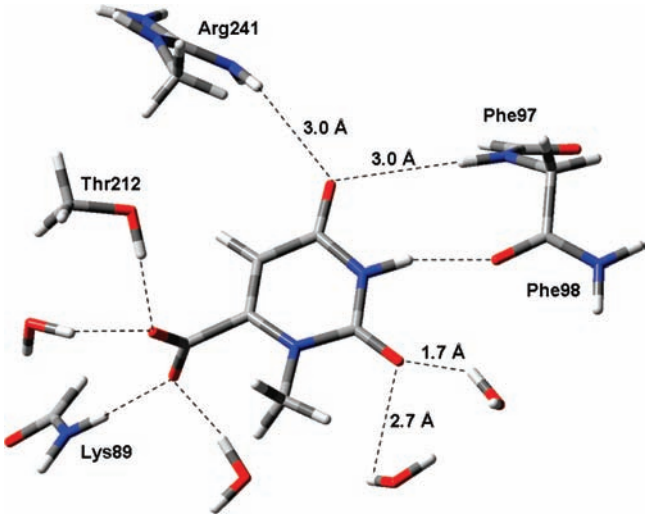

Figure 4. Hydrogen-bond network at the *Pf*OPRT active site. Model was determined in vacuo at the B3LYP/6-31G(d,p) level. The displayed hydrogen-bond distances were used as constraints to match the experimental frequencies shift.

A hydrogen-bond network determined from in vacuo calculations in agreement with experimental values was obtained for distances of C_2═O to two water molecules of 2.4 and 2.7 Å and 3.0 Å for the C_4═O distance from the $NH_2(\omega)$ of Arg241 and the NH of Phe97 (Figure 4). Hydrogen bonds to the 6-carboxyl group include the OH of Thr212, NH of Lys89, and two water molecules. Computed vibrational frequency shifts from this hydrogen-bond network are in agreement with experimental values and the structural model (Table 1). Upon formation of the *Pf*OPRT:1-methyl OA complex, the calculated IR shifts of the carbonyl stretching frequency is -26 cm^{-1} for the C_2═O bond and -44 cm^{-1} for the C_4═O bond (Table 1). The experimentally observed shifts of -20 cm^{-1} for both C═O bonds are smaller than the calculated values because of larger frequency shifts in gas-phase calculations as the result of overestimation of hydrogen-bond interactions. In vacuum, the interactions between the C_4═O bond and the cationic guanidinium of Arg241 tend to be overestimated, giving rise to the significant stretching frequency shift for the C_4═O bond upon binding to the *Pf*OPRT active site. Therefore, calculations were also done to resemble a solvated system.

The hydrogen-bond network was determined in solution using the SCRF method with the Onsager model in Gaussian03. On the basis of the crystal structures, OPRTs are characterized by water-accessible active sites. Thus, geometries were optimized

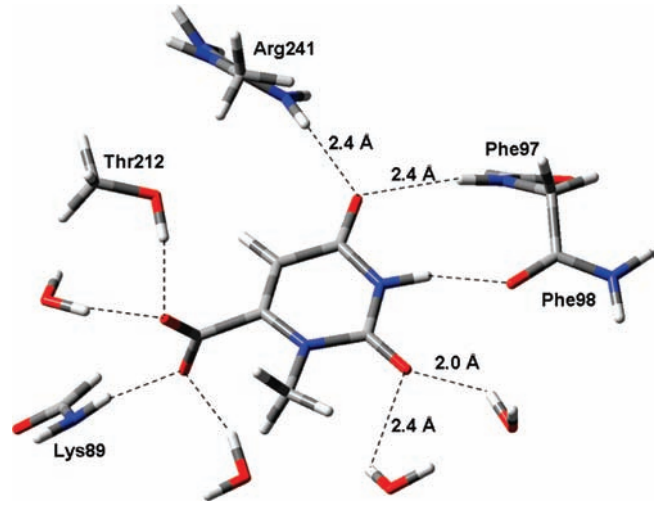

Figure 5. Hydrogen-bond network at the *Pf*OPRT active site determined in water. Model was determined in the dielectric environment of water using the Onsager model implemented in Gaussian 03. The displayed hydrogen-bond distances were used as constraints to match the experimental frequencies shift.

and calculated for vibrational frequencies with the dielectric constant of water. A fixed architecture of the *Pf*OPRT active site was maintained with the distances of C_2═O to two water molecules and C_4═O to the $NH_2(\omega)$ of Arg241 and the NH of Phe97 being iteratively altered to obtain a match to the experimental frequency shifts.

Agreement between calculated and experimental IR frequency shifts was obtained with the C_2═O bond at 2.7 Å from the two ordered water molecules and the C_4═O bond at 2.4 Å from the $NH_2(\omega)$ of Arg241 and the NH of Phe97 (Figure 5). Formation of the Michaelis complex from free 1-methyl OA causes 20 cm^{-1} downward shifts for both C═O stretching frequencies, consistent with observed values (Table 1). Similar to calculations in the gas phase, calculations in water overestimated vibration frequencies by about 7%. This overestimation is due to the neglect of anharmonicity, incomplete description of electron correlation, and imperfect approximation of solvent effects. Despite the need for a scaling correction, calculations including solvent effects give a good match to the observed shifts (Table 1). The observed shifts for ^{13}C labeling in OMPs are about -20 cm^{-1}, indicating a delocalized C═O stretch. The determined hydrogen-bond network shows ^{13}C shifts of -40 cm^{-1} for the C═O stretch with no delocalization (Table 1). Transition-state analysis showed no protonation of OA at the transition state.[11] Combined with the IR-observed polarization of OMP and the calculated polarization of 1-methyl OA, it is implied that the hydrogen-bond network is important for leaving group activation in *Pf*OPRT (see below).

It is also demonstrated that combined FTIR and theoretical calculations can be used to refine the active site structure. Through this approach, the hydrogen-bond network at the *Pf*OPRT active site was proposed. This hydrogen-bond pattern is consistent with those of OPRT homologues, observed from their crystal structures.[13,14,39] For the OPRT family, the conserved hydrogen-bond network indicates an important role in catalysis. The hydrogen-bonding pattern of this conserved network suggests necessary components at the OPRT active site.

Electrostatics of the Orotic Acid Leaving Group. On forming the Michaelis complex with *Pf*OPRT the molecular electrostatic potential surface of 1-methyl OA differs from that in solution

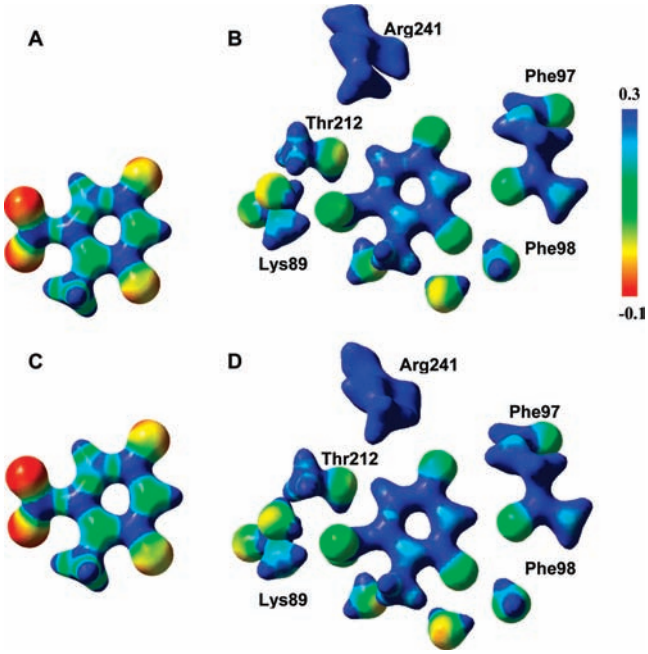

Figure 6. Calculated MEP surfaces. Electron-rich and -deficient atoms are represented by red and blue, respectively. (A) MEP surface of free 1-methyl OA in vacuo. (B) MEP surface of hydrogen-bond network at the *Pf*OPRT catalytic site in vacuo. (C) MEP surface of free 1-methyl OA in water. (D) MEP surface of hydrogen-bond network at the *Pf*OPRT catalytic site in water.

Table 2. Natural Charge of 1-Methyl OA in Solution and in Michaelis Complex[a]

		natural charge	
	atom	free 1-methyl OA	*Pf*OPRT:1-methyl OA
calcd in vacuo	N1	−0.447	−0.431
	O2	−0.676	−0.674
	O4	−0.652	−0.700
	O7	−0.719	−0.721
	O7′	−0.748	−0.739
calcd in water[b]	N1	−0.449	−0.442
	O2	−0.650	−0.686
	O4	−0.649	−0.678
	O7	−0.743	−0.728
	O7′	−0.754	−0.746

[a] NBO analyses were performed on the optimized geometries at the B3LYP/6-31G(d,p) level of theory and basis set. [b] Natural charges in water were determined by the SCRF method using the Onsager model in Gaussian 03.

(Figure 6). Free 1-methyl OA clearly displays electron-rich regions at the 2- and 4-carbonyl groups and the 6-carboxyl group. These groups become less negative (electron-deficient) upon formation of the Michaelis complex as a result of polarization by the surrounding residues and water molecules. The N1 atom, key to the leaving group potential, becomes less negative in the complex and exhibits decreased basicity.

Natural bond order (NBO) analyses were performed on the geometries of free 1-methyl OA and associated hydrogen-bond networks. The natural charges on key atoms are listed in Table 2. Upon formation of the Michaelis complex, the carboxylic oxygen atoms of 1-methyl OA show decreased electronegative potential, a result of the hydrogen-bond and ionic interactions. The cationic guanidinium of Arg241 polarizes the C_4═O bond. NBO analyses in vacuo and in water show reduced negative charge on N1 and decreased C1′−N1 bond strength upon formation of the Michaelis complex.

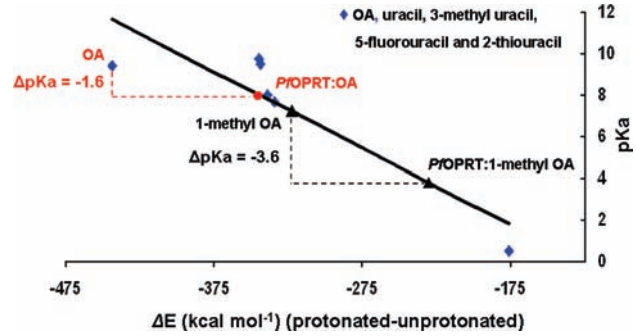

Figure 7. In vacuo computational analysis of the decrease in pK_a at N1 upon formation of the Michaelis complex. Standard curve (♦) was generated by plotting the pK_a values of N1 of OA, uracil, 3-methyl uracil, 5-fluorouracil, and 2-thiouracil versus their corresponding computed zero-point energy difference (ΔE) between protonated and unprotonated state.[35,36] At the *Pf*OPRT catalytic site, pK_a for N1 of OA is decreased by 1.6 compared with free OA in solution (OA → *Pf*OPRT:OA, $\Delta pK_a = -1.6$). 1-Methyl OA is a mimic of OMP. The ΔE value for 1-methyl OA is the energetic difference between 1-methyl OA and demethylated OA ($E_{\text{1-methyl OA}} - (E_{\text{OA, anion}} + E_{\text{methyl, cation}})$). The ΔE value for *Pf*OPRT:1-methyl OA was obtained in the same way. At the *Pf*OPRT catalytic site, pK_a for N1 of 1-methyl OA is decreased by 3.6 compared with free 1-methyl OA in solution (1-methyl OA → *Pf*OPRT:1-methyl OA, $\Delta pK_a = -3.6$).

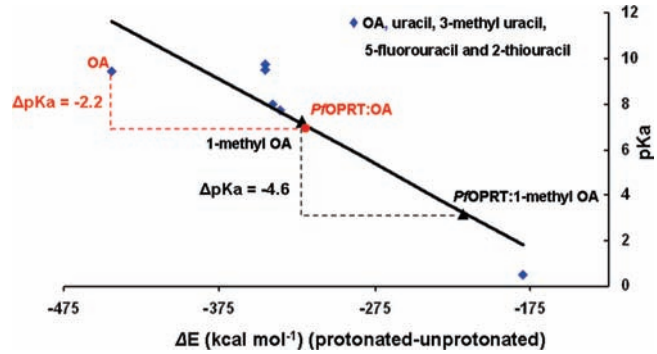

Figure 8. In water computational analysis of the decrease in pK_a at N1 upon formation of the Michaelis complex. Standard curve (♦) was generated by plotting the pK_a values of N1 of OA, uracil, 3-methyl uracil, 5-fluorouracil, and 2-thiouracil versus their corresponding computed zero-point energy difference (ΔE) between protonated and unprotonated state.[35,36] At the *Pf*OPRT catalytic site, pK_a for N1 of OA is decreased by 2.2 compared with free OA in solution (OA → *Pf*OPRT:OA, $\Delta pK_a = -2.2$). 1-Methyl OA is a mimic of OMP. The ΔE value for 1-methyl OA is the energetic difference between 1-methyl OA and demethylated OA ($E_{\text{1-methyl OA}} - (E_{\text{OA, anion}} + E_{\text{methyl, cation}})$). The ΔE value for *Pf*OPRT:1-methyl OA was obtained in the same way. At the *Pf*OPRT catalytic site, pK_a for N1 of 1-methyl OA is decreased by 4.6 compared with free 1-methyl OA (1-methyl OA → *Pf*OPRT:1-methyl OA, $\Delta pK_a = -4.6$).

The polarizing effect of the hydrogen-bond network on N1 of OMP in the Michaelis complex was analyzed computationally. Correlation curves were created by plotting the energetic differences between protonated and unprotonated pyrimidines as a function of their corresponding pK_a values for N1 (Figures 7 and 8).[35,36,40] Zero-point energies of pyrimidines with various protonation states were calculated at the B3LYP/6-31G(d,p) level of theory in vacuo and in water. The pK_a for N1 was analyzed by comparing the energy of 1-methyl OA with OA plus the methyl cation. The energetic difference was used to calculate the pK_a values for N1 in the ground state and the Michaelis complex with reference to the standard curve. The

(40) Versees, W.; Loverix, S.; Vandemeulebroucke, A.; Geerlings, P.; Steyaert, J. *J. Mol. Biol.* **2004**, *338*, 1–6.

ΔpK_a for N1 is −3.6 in response to forming the *Pf*OPRT:1-methyl OA complex (Figure 7). A similar analysis in water shows a ΔpK_a of −4.6 for the N1 atom upon formation of the Michaelis complex. The multiple hydrogen-bond interactions at the *Pf*OPRT active site cause C1′−N1 ground-state destabilization to initiate leaving group activation. Calculations that included the phenyl ring of Phe97 had no effect on the pK_a values. Consequently, it was excluded for computation analysis. However, these are ground-state effects, and the phenyl ring and multiple hydrogen bonds are important in stabilizing the fully dissociated dianionic OA at the *Pf*OPRT transition state.

Leaving group activation through multiple hydrogen-bond and ionic interactions distinguishes *Pf*OPRT from other *N*-ribosyltransferases. Unlike the *Pf*OPRT transition state, most purine *N*-ribosyltransferases transition states feature a protonated leaving group.[26,41−43] Protonation at N7 neutralizes the purine leaving group to facilitate *N*-glycosidic bond cleavage. The ^{13}C-edited FTIR difference spectra and computational analysis for *Pf*OPRT establish leaving group polarization in the Michaelis complex. As a result of the multiple hydrogen bonds to surrounding residues and water molecules, the OA leaving group shows altered atomic charges and potential surface. The anionic 6-carboxyl group interacts with the peptide N−H of Lys89, the side chain OH of Thr212, and two water molecules. The OA leaving group is also polarized through hydrogen-bond interactions with two ordered water molecules around the C_2═O, the peptide C═O of Phe98 near the N_3−H, the guanidinium of Arg241, and the peptide N−H of Phe97 near the C_4═O. The induced change to the OA electrostatic character from these interactions causes decreased basicity at N1 of OA and thereby facilitates loss of the *N*-glycosidic bond. Transition-state analysis from kinetic isotope effects demonstrated dianionic OA at the transition state.[11] The fully dissociated dianionic OA leaving group with delocalized negative charge is proposed to be stabilized by the multiple hydrogen-bond interactions to permit barrier crossing. Thus, activation can also be accomplished through multiple hydrogen-bond interactions, the role of the hydrogen-bond network at the *Pf*OPRT active site.[12]

As the physiological direction of *Pf*OPRT is OMP synthesis, the effect of the hydrogen-bond network on the N1 pK_a of OA was also analyzed. OA has a pK_a of 9.45 for N1 in solution and must be deprotonated for reaction to occur. To understand how N1 is deprotonated, the energetic differences between *Pf*OPRT:OA and *Pf*OPRT-deprotonated OA complexes were calculated for optimized geometries with the same geometric constraints as for the *Pf*OPRT:1-methyl OA complex. The ΔpK_a of N1 on formation of the *Pf*OPRT:OA complex is −1.6 and −2.2 when calculated in vacuo and in water, respectively (Figures 7 and 8). Thus, the catalytic site environment brings the N1 pK_a to the physiological range to facilitate conversion to OMP. The conserved hydrogen-bond network at the *Pf*OPRT active site also plays an important role in creating the nucleophilic form of N1 for attacking C1 of PRPP.

Ionic State of PPi at the *Pf*OPRT Active Site. The ionic state of PPi at the *Pf*OPRT active site was determined by ^{18}O-edited FTIR difference spectra with reference to PPi in solution (Figure 9A−C). The FTIR spectrum of dianionic PPi was obtained at pH 4.5 (Figure 9A). The major band at 1196 cm^{-1} is assigned to the out-of-phase combination of the two asymmetric non-

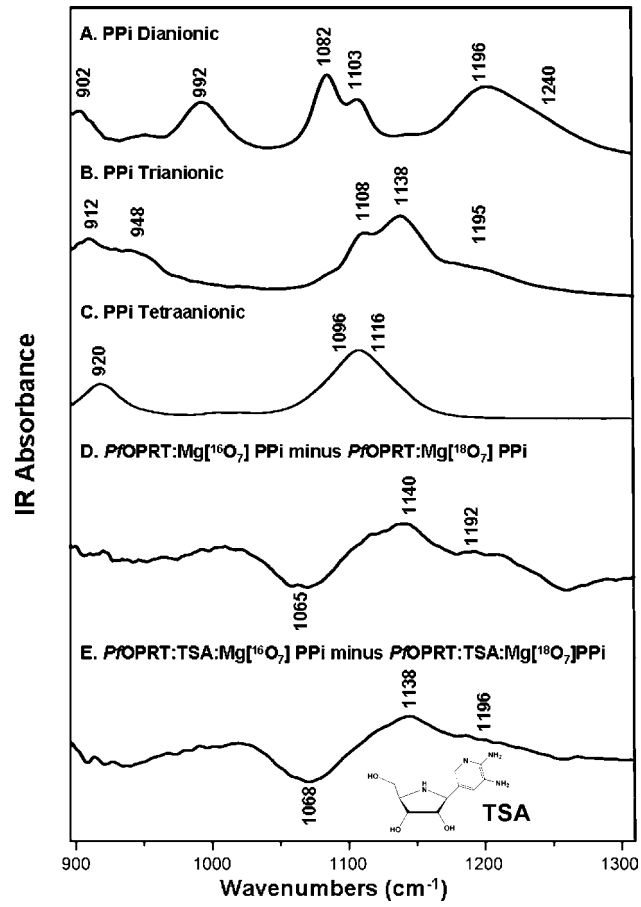

Figure 9. FTIR spectra of free PPi in solution and difference spectra of *Pf*OPRT:MgPPi complexes. (A) FTIR spectrum of 25 mM dianionic PPi (pH 4.5). (B) FTIR spectrum of 25 mM trianionic PPi. The spectrum of trianionic PPi was obtained by subtracting the appropriate amount of A and C from the spectrum of 25 mM PPi at pH 7.5. (C) FTIR spectrum of 25 mM tetraanionic PPi (pH 11). (D) FTIR difference spectrum of *Pf*OPRT:Mg[$^{16}O_7$]PPi minus *Pf*OPRT:Mg[$^{18}O_7$]PPi. Samples were prepared in 50 mM Tris-HCl (pH = 8.0) and 200 mM NaCl. The concentrations of *Pf*OPRT:MgPPi were 3.3:3.3 mM. (E) FTIR difference spectrum of *Pf*OPRT:TSA:Mg[$^{16}O_7$]PPi minus *Pf*OPRT:TSA:Mg[$^{18}O_7$]PPi. Samples were prepared in 50 mM Tris-HCl (pH = 8.0) and 200 mM NaCl. The concentrations of *Pf*OPRT:TSA:MgPPi were 3.3:3.3:3.3 mM.

bridging P••O bond stretches. The shoulder band at 1240 cm^{-1} is assigned to an asymmetric combination of the nonbridging P••O bond stretches. The major band at 1082 cm^{-1} is assigned to an asymmetric combination of the two P−OH bond stretches. The band at 1103 cm^{-1} is assigned to the in-phase combination of the two symmetric nonbridging P••O bond stretches. The IR band at 902 cm^{-1} is assigned to the asymmetric bridging P−O bond stretches. The assignments of IR bands are based on previously reported results[16] and also supported by the theoretical calculations (see below).

The FTIR spectrum of tetraanionic PPi was obtained at pH 11 (Figure 9C). The major IR bands at 1096 and 1116 cm^{-1} are assigned to the asymmetric combinations of the nonbridging P••O bond stretches, and the 920 cm^{-1} band is assigned to the asymmetric bridging P−O bond stretches. The FTIR spectrum of trianionic PPi was obtained at pH 7.5 where more than 80% of PPi exists as the trianion (pK_a values of PPi are 0.9, 2.1, 6.7, and 9.3). The IR spectrum of trianionic PPi was obtained by subtracting appropriate fractions of the di- and tetraanionic PPi IR spectra from that at pH 7.5 (Figure 9B). The major IR bands at 1108, 1138, and 1195 cm^{-1} are assigned to the asymmetric

(41) Lewandowicz, A.; Schramm, V. L. *Biochemistry* **2004**, *43*, 1458–1468.
(42) Luo, M.; Li, L.; Schramm, V. L. *Biochemistry* **2008**, *47*, 2565–2576.
(43) Singh, V.; Luo, M.; Brown, R. L.; Norris, G. E.; Schramm, V. L. *J. Am. Chem. Soc.* **2007**, *129*, 13831–13833.

Table 3. Experimental and Computational Nonbridging P··O Stretching Frequencies[a]

		P··O stretching frequencies (cm^{-1})		
		υ_{a1}	υ_{a2}	υ_{a3}
expt	$P_2O_7H_2^{2-}$	1196		1240
	$P_2O_7H^{3-}$	1108	1138	1195
	$P_2O_7^{4-}$	1096	1116	
	*Pf*OPRT:MgPPi		1140	1192
	*Pf*OPRT:TSA:MgPPi		1138	1196
calcd[b]	$P_2O_7H_2^{2-}$	1074	1244	1248
	$P_2O_7H^{3-}$	1094	1159	1182
	$P_2O_7^{4-}$	1060	1078	1079

[a] υ_as are the asymmetric combination of nonbridging P··O stretches observed in FTIR spectra or determined through quantum chemical calculations. [b] Vibrational frequencies for di-, tri-, and tetraanionic PPi were calculated on the optimized geometry at the B3LYP/6-31G(d,p) level using Gaussian 03.

combinations of the nonbridging P··O bond stretches, and the band at 912 cm^{-1} is assigned to the asymmetric bridging P−O bond stretches. Chelation of PPi with Mg^{2+} in solution results in a small upward shift (12 cm^{-1}) with no other effect on the IR spectra. Binding of Mg^{2+} to PPi causes decreased pK_a values (pK_{a3} = 4.4 and pK_{a4} = 6.6).[44] FTIR spectra of $Mg^{2+}H_2P_2O_7^{2-}$, $Mg^{2+}HP_2O_7^{3-}$, and $Mg^{2+}P_2O_7^{4-}$ were therefore measured at pH 3.3, 5.5, and 9.0, respectively (see Supporting Information).

Vibrational frequency calculations for PPi at varied ionic states were performed in vacuo at the B3LYP/6-31G(d,p) level of theory and basis set and compared with values from the FTIR spectra (Table 3). Calculated frequencies for dianionic PPi show asymmetric nonbridging P··O bond stretches at 1074, 1244, and 1248 cm^{-1} with the observed asymmetric stretch mode about 120 cm^{-1} higher than the 1074 cm^{-1} calculation. For tri- and tetraanionic PPi, the calculated frequencies for asymmetric nonbridging P··O bond stretches are in agreement with the experimental values.

The ionic state of PPi at the *Pf*OPRT active site was determined from the ^{18}O-edited FTIR difference spectra for the binary complex of *Pf*OPRT·MgPPi and the ternary complex of *Pf*OPRT·MgPPi·transition-state analogue (TSA) (Figure 9D and 9E). The FTIR difference spectra of these complexes are similar, with the major IR bands for unlabeled PPi around 1139 and 1195 cm^{-1}. Compared to the FTIR spectra of free PPi and MgPPi in solution (see Supporting Information for free PPi spectra at pH 8.0), the band frequencies and profiles of the FTIR difference spectra support a trianionic PPi nucleophile in both complexes. In solution at pH 8.0, MgPPi exists as $Mg^{2+}P_2O_7^{4-}$ due to the decreased pK_{a4} caused by Mg^{2+} binding. At the *Pf*OPRT active site, the octahedral coordination adopted by Mg^{2+} tends to weaken its effect on the pK_a decrease for PPi. Consequently, at the experimental pH, a trianionic PPi ($Mg^{2+}PPi^{3-}$) is found at the *Pf*OPRT active site. The broad IR bands indicate no strong hydrogen-bond interactions between active site residues and PPi. Figure 9E shows the structure of a proposed TSA (K_i = 450 nM) of *Pf*OPRT.[45] The geometry of complexes with bound transition-state analogues is proposed to resemble a point on the reaction coordinate with features similar to the transition state. The ^{18}O-edited FTIR difference spectra in this complex is largely unchanged from that of the binary *Pf*OPRT·MgPPi complex. Thus, in both the binary and the ternary complexes, the similar broad IR bands indicate no strong electrostatic and/or hydrogen-bond interactions imposed on the PPi nucleophile by the enzyme. For the ternary complex with features of the transition state, the bound PPi nucleophile shows no additional P··O bond polarization, suggesting that the approach to the transition state is dominated by leaving group activation rather than nucleophile polarization. While the activated OA leaving group is stabilized by the multiple hydrogen bonds, the PPi nucleophile is immobilized at the active site without polarized P··O bonds. This pattern is known from other *N*-ribosyl transferases and supports a catalytic mechanism proceeding through ribocation migration toward the PPi nucleophile following formation of the transition state.[46]

The electronic state of PPi at the catalytic site distinguishes *Pf*OPRT from human HGPRT where bound MgPPi exists as a tetraanionic nucleophile.[16] No significant P··O bond polarization is observed at either the *Pf*OPRT or human HGPRT active sites, suggesting similar catalytic mechanisms involving migration of the ribocation toward the MgPPi with minimal nucleophilic participation at the transition state. Unlike *Pf*OPRT and human HGPRT, human PNP in complex with phosphate and the transition-state analogue immucillin-H is characterized by a dianionic phosphate with strongly distorted P··O bonds.[15] The mechanism of phosphate distortion in human PNP involves contributions from both the protein and the hydrogen bonding of the phosphate to bound substrate or transition-state analogues.[17] In HGPRT and yeast OPRT structures, a magnesium ion chelated to the pyrophosphate is coordinated to the nucleoside hydroxyl groups, consistent with the observed lack of pyrophosphate bond change in Michaelis or transition-state complexes.

Reaction Coordinate for *Pf*OPRT. Isotope-edited FTIR difference spectra with OMP combined with homology modeling and computational analysis establishes ground-state destabilization. Combined with knowledge of the transition state,[12] the result establishes a reaction coordinate with leaving group activation by multiple hydrogen-bond interactions but without protonation prior to or at the transition state. The undistorted trianionic PPi nucleophile shows no significant P··O bond polarization at the *Pf*OPRT catalytic site and indicates the reaction is ribocation driven and its nucleophilic capture involves 'nucleophilic displacement by electrophile migration'[46] (Figure 10). Upon binding to the *Pf*OPRT active site, the orotate group of OMP rotates about 110° anticlockwise around the C1′−N1 bond (from its optimal position calculated in vacuo) to form multiple hydrogen bonds with active site residues and water molecules (Figure 10). In the Michaelis complex, the extended hydrogen-bond network results in decreased basicity at N1 of OMP to weaken the *N*-ribosidic bond and promote activation of the OA leaving group. On the basis of measured kinetic isotope effects, transition-state analyses of *Pf*OPRT with substrate analogues suggest a late transition state for *Pf*OPRT with OMP and PPi.[11,12] Unlike early transition states with partial bonds to leaving groups, the late *Pf*OPRT transition state is characterized by fully dissociated dianionic OA, well-developed ribocation, and weak PPi nucleophilic participation. The fully dissociated OA dianion is stabilized by multiple hydrogen bonds. In this reaction coordinate, the ribocation migrates toward $Mg^{2+}PPi^{3-}$ to complete the reaction. Beyond the transition state,

(44) Boskey, A. L.; Posner, A. S. *J. Phys. Chem.* **1973**, *77*, 2313–2317.
(45) Furneaux, R. H.; Schramm, V. L.; Tyler, P. C. *Bioorg. Med. Chem.* **1999**, *7*, 2599–2606.
(46) Schramm, V. L.; Shi, W. *Curr. Opin. Struct. Biol.* **2001**, *11*, 657–665.

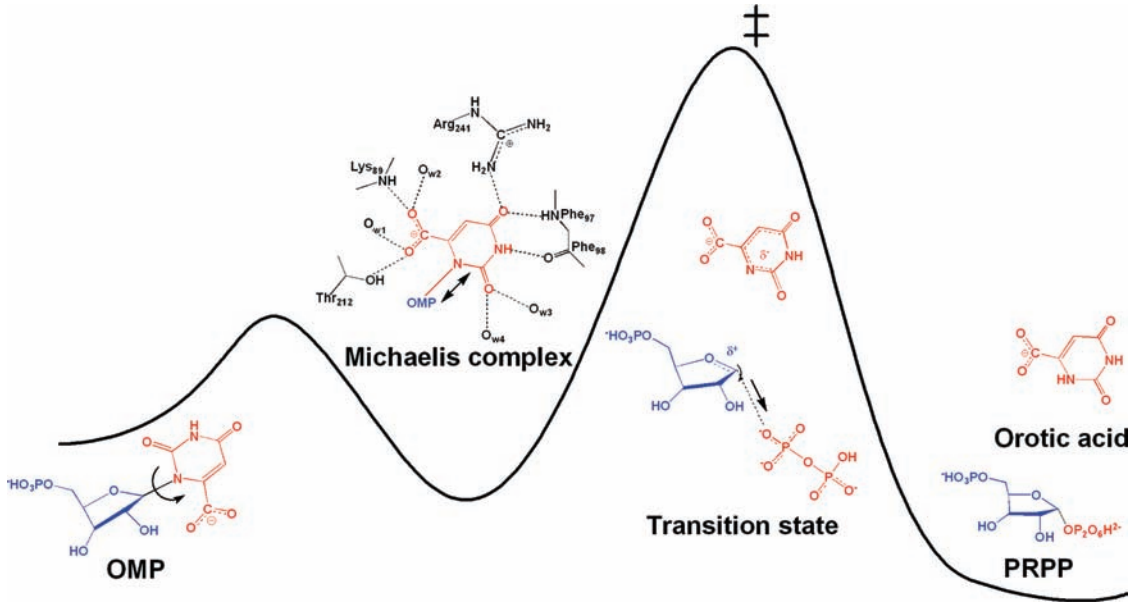

Figure 10. Proposed reaction coordinate of *Pf*OPRT-catalyzed pyrophosphorolysis of OMP. The relative energy along the reaction coordinate is arbitrary with the highest energetic point as the transition state. The first energetic local minimum represents formation of the Michaelis complex. Chemical structure in each step is shown with the arrow indicating the direction of moiety rotation or migration. Hydrogen-bond network surrounding orotate in the Michaelis complex is highlighted.

the ribocation is captured to form MgPRPP and the products are released from the active site.

Conclusion

FTIR difference spectra reveal large downward shifts of 20 cm^{-1} for C═O carbonyl stretching frequencies for OMP in the Michaelis complex, indicating formation of strong hydrogen bonds between active site residues and the orotate base. Crystal structures of OPRT homologues reveal that the enzyme undergoes large conformational change associated with the substrates and products binding.[13,14,38,39] The conformational transition induced by binding is believed to create the interactions between enzyme and reactants for catalysis. Through these active site interactions and conformational movements, the OPRT enzyme lowers the energy barrier and destabilizes substrate toward the formation of products. We can postulate that enzymatic motions coupled to the multiple H-bonds and in the presence of bound $Mg^{2+}PPi^{3-}$ form the reaction coordinate. Specific leaving group activation mechanisms predict that ribosyl substrates with activated leaving groups (*p*-nitrophenyl-*β*-D-ribose 5′-phosphate) will be poor substrates, and this has been reported for *Pf*OPRT.[11] The *Pf*OPRT homology structure predicted an active site hydrogen-bond network that was computationally matched to the IR vibrational shifts to cause decreased basicity at N1 of OMP, supporting a reaction coordinate with leaving group activation by multiple hydrogen-bond interactions. ^{18}O-Edited FTIR difference spectra of *Pf*OPRT·MgPPi·TSA revealed a trianionic PPi nucleophile at the *Pf*OPRT active site with no significant P··O bond polarization, supporting a mechanism proceeding through ribocation migration toward the $Mg^{2+}PPi^{3-}$ nucleophile. Together with transition-state analyses, isotope-edited IR results establish a reaction coordinate for *Pf*OPRT-catalyzed OMP pyrophosphorolysis.

Acknowledgment. We thank Drs. Richard H. Furneaux and Peter C. Tyler (Industrial Research Ltd., New Zealand) for synthesis of the transition-state analogue inhibitor. We thank Dr. Hui Xiao (The Laboratory for Macromolecular Analysis & Proteomics, Albert Einstein College of Medicine) for the mass spectral measurements. We also thank Prof. Jiali Gao of the University of Minnesota Supercomputer Institute for computer time. This work was supported in part by research grants EB001958 (H.D.), AI049512, and GM041916 (V.L.S.) from the NIH.

Supporting Information Available: Full author list of ref 31 and complete calculation results. This material is available free of charge via the Internet at http://pubs.acs.org.

JA107806J